



# Insights into dry reforming of methane over nickel catalyst using a thermodynamic model

Rakhi<sup>1</sup> · Vivien Günther<sup>2</sup> · Fabian Mauss<sup>1</sup>

Received: 24 March 2023 / Accepted: 17 May 2023 / Published online: 3 June 2023  
© The Author(s) 2023

## Abstract

A thermodynamic model is developed using a one-dimensional model, LOGEcat to understand the dry reforming of methane over nickel-based catalysts. To do so, we have extended our previously developed mechanism (Rakhi and Shrestha in *React Kinet, Mech Catal* 135:3059–3083, 2022) which contains 21 reversible reactions by adding 5 more reversible reactions and updating the thermochemistry of one intermediate species. The adjusted mechanism contains 26 reversible reactions obtained with the help of thermodynamic analysis. This study focuses on using the thermodynamic model for dry reforming of methane and insights into the reaction pathways and sensitivity analysis for the kinetically consistent surface reaction mechanism. The applicability of the mechanism is examined for reactor conditions in terms of parameters such as temperature by comparing the results with the available reference data. The mechanism is able to accurately express the reforming conditions of methane over the nickel catalyst for complete range of temperature and also provide useful insights into the reaction pathways established with the thermodynamic model.

**Keywords** Nickel-based catalyst · Kinetic consistency · Thermodynamic analysis · Dry reforming · 1D modelling

---

✉ Rakhi  
rakhi.rakhi@b-tu.de

Vivien Günther  
Vivien.Guenther@logesoft.com

Fabian Mauss  
maussf@b-tu.de

<sup>1</sup> BTU Cottbus-Senftenberg, 03046 Cottbus, Germany

<sup>2</sup> LOGE AB, 03044 Cottbus, Germany

## Introduction

The most common catalytic technologies for converting natural gas to synthesis gas in various compositions involves processes, for instance, steam reforming (SR), partial oxidation (POX), autothermal reforming (ATR), and dry reforming (DR) [1, 2]. These processes have been considered in literature, such as, SR in [1–3, 3–5], DR in [5–7], CPOX in [8–12].

All these processes suffer coke formation at different conditions and the deposition of coke on catalysts and reactor pipe walls are serious problems in many industrial reactors that involve methane as fuel leading to the blockage of reactor tube. This can also physically disintegrate catalyst structure [13–17]. One of the mitigating measure to reduce the coke formation is proposed by Blekkan et al. [16] where the dry reforming of methane can be investigated at higher pressures and temperatures by using hydrogen and water as co-feed. Pure dry reforming process would produce very hydrogen deficient syngas and does not lead to net consumption of CO<sub>2</sub> without an external source of hydrogen when thermodynamics and process efficiencies are taken into account.

Further investigations are needed to understand and reduce the coke formation problem with different fuel ratio which also demands a better understanding of the processes of catalytic oxidation and reforming of methane at a molecular level. Various kinetic models are proposed in literature and the elementary steps involved in the reaction mechanism have been investigated in [1, 3, 7, 18–21]. Despite all these studies, the detailed path for the conversion of methane to syngas and carbon remains a controversial issue [22].

Another problem in setting up a reaction mechanism is due to the difficulty to define the thermodynamic data for intermediate surface species. Hence, most of the mechanisms available in literature are kinetic models which uses the kinetic parameters for forward and backward reactions making the mechanism thermodynamically consistent. These mechanisms do not use the thermochemistry of the species.

In this paper, a thermodynamic model is used to understand the dry reforming of methane over a nickel catalyst. Further, a detailed sensitivity analysis of reactions and reaction pathways for the thermodynamic model is analysed and the major differences are noted between the available kinetic schemes and the used thermodynamic model after a successful validation of the model by comparing the simulation results with the literature [23] for various inlet gas compositions in a wide temperature range. In future, the model can be applied to check the fuel ratio limit to mitigate the coke formation problem.

## Surface reaction mechanism

Methane is converted into a mixture of hydrogen, carbon monoxide, and carbon dioxide via different molecular paths indicated as an overall reaction [23] and Delgado et al. [23] developed a detailed surface reaction mechanism using the

overall/global reactions to model the various reforming processes which covers all the ways from total oxidation to pyrolysis. Their kinetic scheme consists of 52 reactions with 6 gas-phase and 14 surface species.

In the present study, a thermodynamic model is developed taking the mechanism from Delgado et al. [23] as base. This work is also an extension of our previously developed surface reaction mechanism [24] which comprises of 21 reactions by adding new reaction scheme involving carboxyl species as intermediate along with carbon formation paths. Our previous mechanism [24] was limited only for steam reforming of methane over nickel, however, the developed mechanism in the present investigation is also applicable to oxidative and dry reforming along with steam reforming. In this paper, our focus is only to discuss dry reforming process in detail and the other reforming processes will be discussed in a separate paper.

The thermodynamic model consists of 26 reactions in total with 7 gas-phase and 14 surface species. The set of 21 reactions have been directly taken from Rakhi et al. [24] and only 5 more reversible reactions have been added here and these reactions are taken from Delgado et al. [23], summarized in Table 1. Therefore, the kinetic data remains same as Delgado et al. [23] and the thermodynamic data is taken from Rakhi et al. [24]. The thermochemistry of the new species, COOH(s) is taken from Liu et al. [25].

## Simulation set-up

The thermodynamic model is developed with the help of a one-dimensional tool, LOGEcat [26]. The model is a part of the LOFESoft software suite for chemical reaction calculations and a complete description of the model is omitted to avoid repetition and is given in our previous publication [24]. The pressure gradient along the inhomogeneity of the mixture is neglected due to the small diameter of the catalytic channel and the external diffusion is modeled by a separate pore gas zone close to the wall. The model is based on the single-channel 1D catalyst model where the single channel is divided into a finite number of cells with each cell treated as a perfectly stirred reactor (PSR).

A single layer of washcoat is used to perform the simulations with the reactor consisting of a circular catalyst of radius 5 mm and a reaction zone of 27 mm length.

**Table 1** The new reaction pathways added to Rakhi et al. [24].  $A_r$  is the pre-exponential factor,  $E_r$  is the activation energy and  $\beta_r$  is the temperature exponent

Rx	Reaction	$A_r$ (cm,mol,s)	$E_r$ (kJ/mol)	$\beta_r$ (-)
R1	$\text{CO(s)} + \text{H(s)} = \text{C(s)} + \text{OH(s)}$	$3.522 \times 10^{+18}$	105.5	- 0.2
R2	$2\text{CO(s)} = \text{C(s)} + \text{CO}_2\text{(s)}$	$1.624 \times 10^{+14}$	241.8	0.5
R3	$\text{CO(s)} + \text{OH(s)} = \text{COOH(s)} + \text{Ni(s)}$	$6.003 \times 10^{+20}$	97.6	0.2
R4	$\text{CO}_2\text{(s)} + \text{H(s)} = \text{COOH(s)} + \text{Ni(s)}$	$6.250 \times 10^{+24}$	117.3	- 0.5
R5	$\text{H(s)} + \text{COOH(s)} = \text{HCO(s)} + \text{OH(s)}$	$6.000 \times 10^{+22}$	104.9	- 1.2

We have used the geometric data and catalyst parameters same as the reference paper [23]. The surface area per catalyst length is adjusted by a sensitivity analysis. Nitrogen dilution is nearly 96% and the surface site density,  $\tau$  for Ni is  $2.6 \times 10^{-5}$  mol/m<sup>2</sup>.

As done by Delgado et al. [23] for the kinetic model, the simulations are performed at 4 slpm (standard liters per minute, T=298.15 K and p=1.01325 bar) for our thermodynamic model. The reaction temperatures are varied in a range [400–1200] K for various reactor conditions. Three cases have been considered for the analysis in the chosen temperature range while keeping all the other parameters constant. The inlet gas composition is varying for all the cases summarized in Table 2. The simulation results for these cases, i.e., DR as well as DR with hydrogen and water as co-feed over a Ni-coated monolithic catalyst, are discussed in next section and the applicability of the thermodynamic model developed in this study is tested by comparing the simulation results with literature.

## Methane dry reforming (DR)

The developed mechanism with 26 reversible reactions is utilized to check the predictability of the model for dry reforming, i.e., methane reforming with CO<sub>2</sub>. The concentration of gas-phase species, CH<sub>4</sub>, CO<sub>2</sub>, H<sub>2</sub>, CO and H<sub>2</sub>O, computed with our model at the reactor outlet as a function of temperature along with the reference data from Delgado et al. [23] is displayed in Fig. 1.

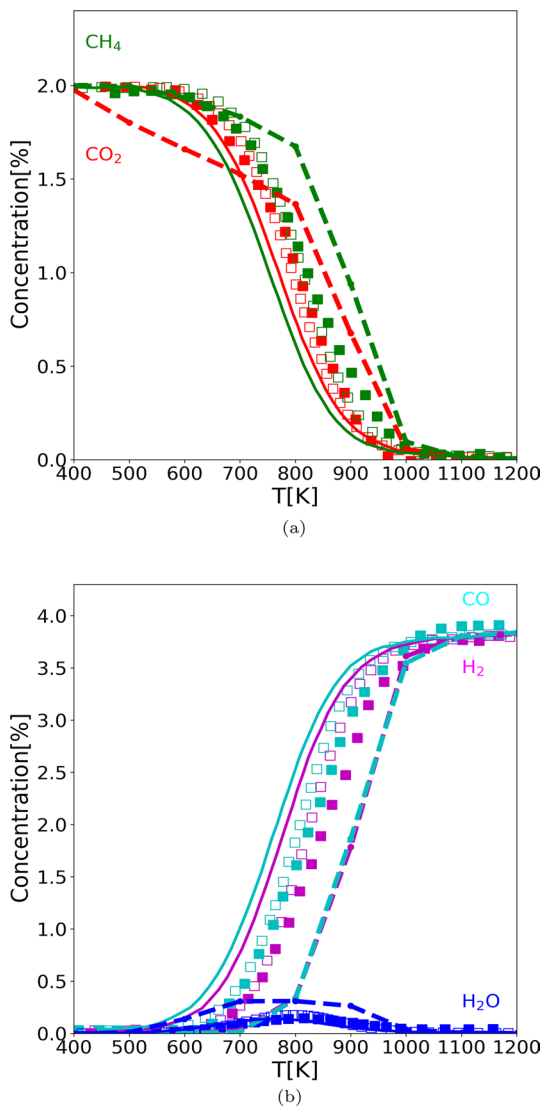
Both the reactants are shown in Fig. 1a, i.e., methane and carbon dioxide concentration, computed with the LOGEcat. Note that the reactant consumption starts at  $\approx 600$  K and as expected, the concentration for both the reactants decreases with increasing temperature similar to the reference data. A full consumption of CH<sub>4</sub> as well CO<sub>2</sub> happens at temperature  $\approx 1000$ K.

The reforming with the thermodynamic model is slightly away from the kinetic model which is very close to the equilibrium calculations for the considered reforming conditions. The deviations in the species concentration with the thermodynamic model can be explained by looking into the reactions sensitivity analysis and the

**Table 2** Summary of the simulation cases as dry reforming (DR), DR with hydrogen as co-feed (DR\_H<sub>2</sub>), and DR with water as co-feed (DR\_H<sub>2</sub>O). The temperature used to perform the simulations is varied in the range [400–1200] K for each case given below. The inlet composition of the species is given in volume %

Case	DR	DR_H <sub>2</sub>	DR_H <sub>2</sub> O
Fuel composition	CH <sub>4</sub> /CO <sub>2</sub>	CH <sub>4</sub> /CO <sub>2</sub> /H <sub>2</sub>	CH <sub>4</sub> /CO <sub>2</sub> /H <sub>2</sub> O
CH <sub>4</sub> (vol. %)	2.00	1.62	1.67
H <sub>2</sub> O (vol. %)	–	–	2.13
CO <sub>2</sub> (vol. %)	2.00	2.08	2.13
H <sub>2</sub> (vol. %)	–	1.80	–
N <sub>2</sub> (vol. %)	96.00	94.50	94.07

**Fig. 1** The concentration of **a** reactants and **b** products for dry reforming are shown as a function of temperature along with the reference data from Delgado et al. [23]. The unfilled squares represents reference simulations, filled squares: reference experiments, solid lines: reference equilibrium calculations and dash lines: LOGEcat calculations with the thermodynamic model



reaction pathways followed for consumption of methane and carbon dioxide along with the formation of the product species and will be discussed shortly.

Fig. 1b illustrates the concentration of the products, H<sub>2</sub>, CO and H<sub>2</sub>O. With the consumption of CH<sub>4</sub> and CO<sub>2</sub>, a gradual increase in the formation of H<sub>2</sub> and CO is noted in the whole temperature range, leading to the thermodynamic equilibrium for temperatures above 1000 K.

The computed water concentration in Fig. 1b shows increase in the concentration profile in temperature range 400–700 K reaching a maximum at around 800 K and then starts to decrease with increasing temperature. The qualitative behaviour of

this species matches with the reference data for the developed mechanism, however, overall the thermodynamic model over-predicted the species concentrations almost by a factor of two in case of dry reforming of methane. This hints towards the indirect path for formation of  $H_2$  and CO through  $H_2O$  whereas, a direct oxidation is followed for the kinetic model.

The gas-phase species concentration predicted with the thermodynamic model shows deviation compared to the reference data in the considered temperature range. Hence, we next show the reaction pathways in Figs. 2 and 3 for steam-, dry-reforming as well as partial oxidation based on C-atom and H-atom flow, respectively, at a temperature higher than the ignition temperature, 1073 K, in order to understand the differences between computed and reference results.

The formation of  $CO_2$  gas-phase species based on C-atom (Fig. 2) at 1073 K is maximum via direct route through  $CO(s)$  to  $CO_2(s)$ , i.e.,  $\approx 50\%$  for SR and  $\approx 86\%$  for CPOX, and using indirect route from  $COOH(s)$  is  $\approx 13\%$  for SR and  $0.4\%$  for CPOX, whereas, the formation of CO gas-phase species from  $CO(s)$  is  $\approx 36\%$  for SR and  $\approx 14\%$  for CPOX. However, for the DR,  $CO_2$  is used as an inlet gas and is being used which leads to the 100% formation of CO gas-phase species displayed in the figure. Note that the reaction pathways are temperature dependent and the

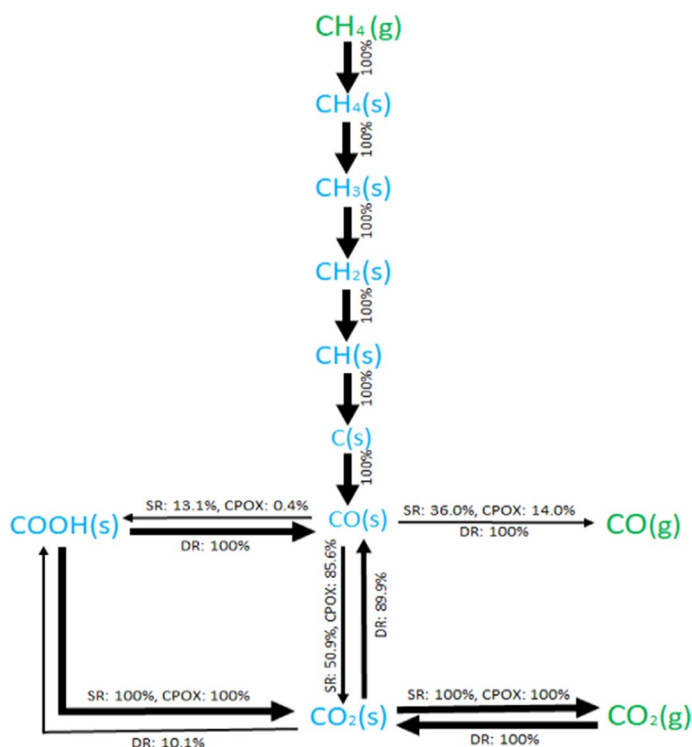


**Fig. 2** Reaction flow analysis for steam reforming (SR), catalytic partial oxidation (CPOX) and dry reforming (DR) of methane on nickel for constant fuel ratio and pressure at 1073 K based on C-atom

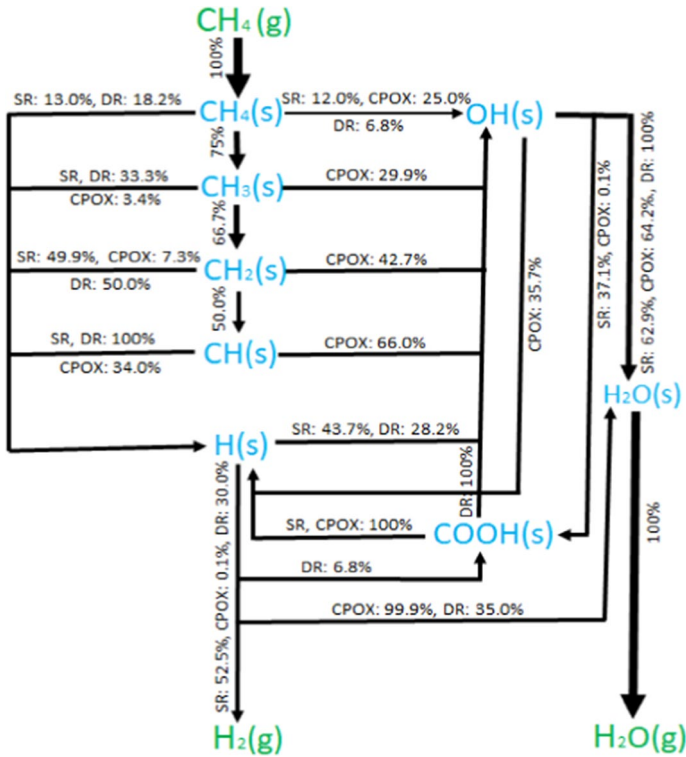


**Fig. 3** Reaction flow analysis for the same processes and at the same conditions as previous figure based on H-atom

formation of these gas-phase species might behave differently with varying temperatures. Based on H-atom (Fig. 3), the reaction pathways for SR, CPOX and DR are also changing. In case of DR, formation of OH(s) takes place from H(s) to COOH(s) route whereas SR and CPOX follows the reverse path and leads to the formation of H(s) from OH(s) through COOH(s). In case of CPOX, direct formation of H(s) from OH(s) also happens without using intermediate COOH(s).

The most sensitive reactions from the developed mechanism for methane conversion by different methods considered, for instance, steam reforming, dry reforming and partial oxidation are shown in Fig. 4. The sensitive analysis is performed at same conditions as mentioned in Fig. 2. Similar to the reference results [23], CH<sub>4</sub> conversion by oxygen assisted methane dehydrogenation given by R11 as CH<sub>4</sub>(s) + O(s) = CH<sub>3</sub>(s) + OH(s) is a sensitive step for all processes (DR, SR and CPOX) at 1073 K particularly for CPOX. However, methane dehydrogenation by R7 (CH<sub>4</sub>(s) + Ni(s) = CH<sub>3</sub>(s) + H(s)) is important only in SR and DR and not for CPOX of methane. The desorption of CO by R5 (CO(s) = CO + Ni(s)) is sensitive only for DR and methane dehydrogenation by R8 (CH<sub>3</sub>(s) + Ni(s) = CH<sub>2</sub>(s)) is only sensitive for SR. For CPOX, R2 (2O(s) = O<sub>2</sub> + 2Ni(s)), R12 (CH<sub>3</sub>(s)

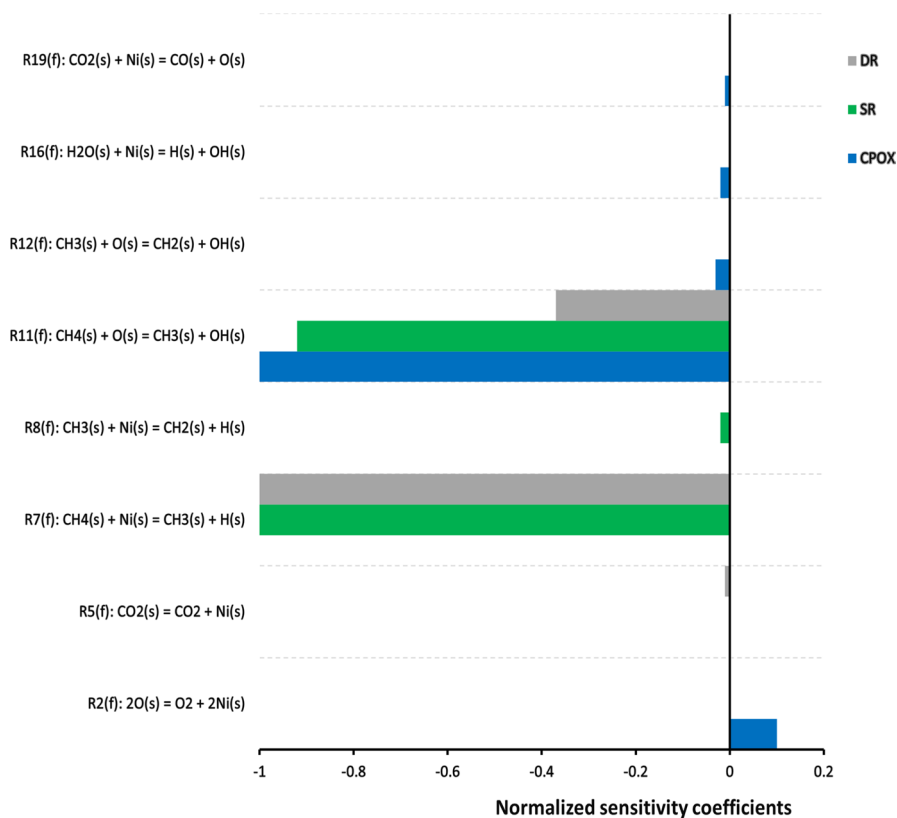


**Fig. 4** Sensitivity coefficients of  $\text{CH}_4$  at 1073 K for SR, DR and CPOX conditions

+  $\text{O}(\text{s}) = \text{CH}_2(\text{s}) + \text{OH}(\text{s})$ , R16 ( $\text{H}(\text{s}) + \text{O}(\text{s}) = \text{OH}(\text{s}) + \text{Ni}(\text{s})$ ) and R19 ( $\text{CO}(\text{s}) + \text{H}(\text{s}) = \text{C}(\text{s}) + \text{OH}(\text{s})$ ) are also slightly sensitive.

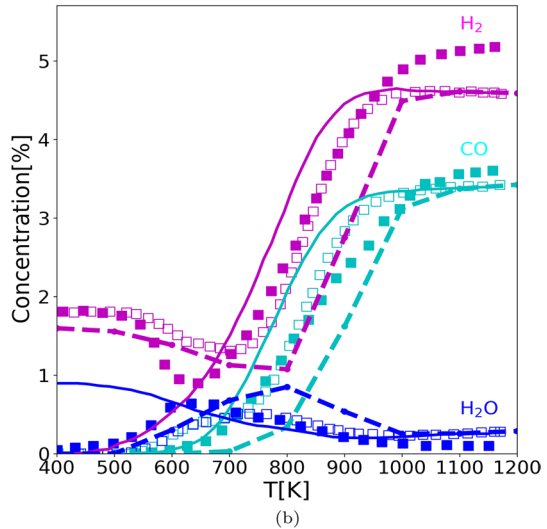
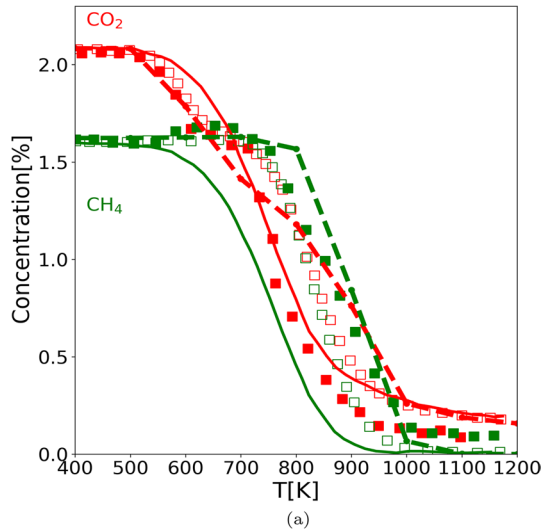
## Effect of hydrogen and water on DR

The coke deposition on catalysts and the reactor pipe walls is a major issue with reactors using methane as fuel and this can lead to even complete catalyst deactivation or lower catalytic activity depending on the amount of solid carbon deposited on the catalyst surface [13–16]. Blekkan et al. investigated dry reforming of methane at higher pressures and temperatures by co-feeding hydrogen and water as inhibitors of coke formation.

So, in order to check the predictability of the thermodynamic model and impact of reactions of the new surface reaction mechanism developed in this study, we have further performed the simulations utilizing  $\text{H}_2$  and  $\text{H}_2\text{O}$  as inhibitors in methane reforming with  $\text{CO}_2$ . The influence of  $\text{H}_2$  and  $\text{H}_2\text{O}$  is shown in Figs. 5 and 6, respectively. In both the figures, (a) shows the computed reactant species concentration



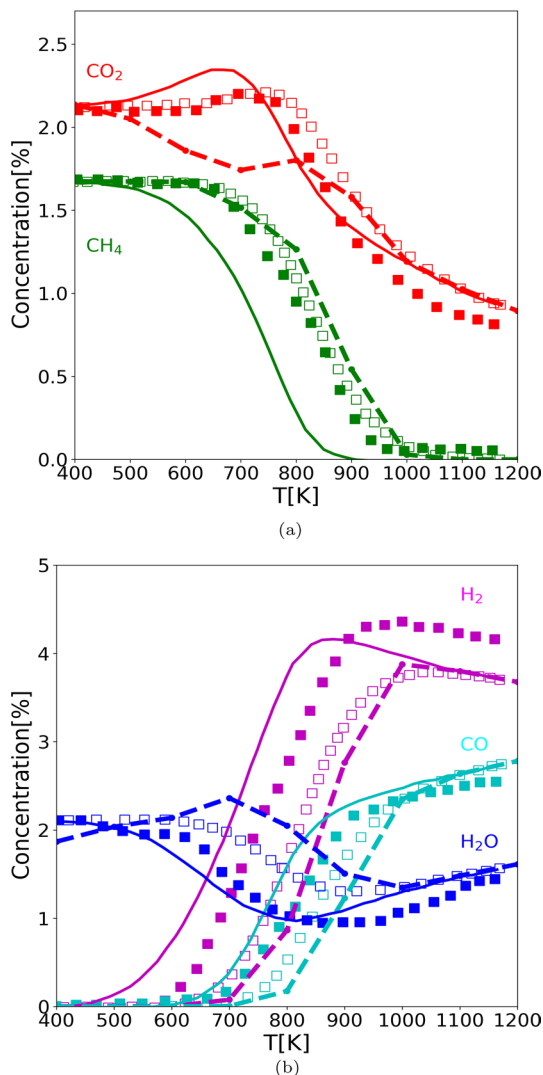
**Fig. 5** **a**  $\text{CH}_4$  and  $\text{CO}_2$ , **b**  $\text{H}_2$ ,  $\text{CO}$  and  $\text{H}_2\text{O}$  concentration as a function of temperature for catalytic dry reforming of methane with co-feed  $\text{H}_2$  for fixed inlet gas composition and pressure along with the reference data from Delgado et al. [23]. The unfilled squares represents reference simulations, filled squares: reference experiments, solid lines: reference equilibrium calculations and dash lines: LOGEcat calculations with the thermodynamic model



and (b) depicts the concentration of product species using LOGEcat. We have used the same simulating conditions as given in Delgado et al. [23].

The consumption of  $\text{CO}_2$  species profile for dry reforming (Fig. 1a) and co-feed  $\text{H}_2$  (Fig. 5a) are gradually decreasing with temperature increase. For dry reforming the full consumption of reactant species is noted at 1000 K whereas for co-feed  $\text{H}_2\text{O}$ , the consumption stops at around 700 K and then this species starts to form with increasing temperature. With the co-feed  $\text{H}_2\text{O}$  (Fig. 6b), the variation of the concentration of this species as a function of temperature is different and there is formation of the species in medium temperature range for the present case as well as for the reference data considered for comparison.

**Fig. 6** **a**  $\text{CH}_4$  and  $\text{CO}_2$ , **b**  $\text{H}_2$ ,  $\text{CO}$  and  $\text{H}_2\text{O}$  concentration as a function of temperature for catalytic dry reforming of methane with co-feed  $\text{H}_2\text{O}$  while keeping all other parameters constant along with the reference data from Delgado et al. [23]. The unfilled squares represents reference simulations, filled squares: reference experiments, solid lines: reference equilibrium calculations and dash lines: LOGEcat calculations with the thermodynamic model



The formation of  $\text{H}_2$  gas-phase species for dry reforming as well as  $\text{H}_2\text{O}$  co-feed (Fig. 1b and Fig. 6b) starts at around 700 K and increases with temperature increase until thermodynamic equilibrium is reached. Whereas for  $\text{H}_2$  co-feed, Fig. 5b, a drop is observed indicating the consumption of the species in temperature range 400–800 K. From 800 K, formation of the species shows same qualitative behaviour as other two cases and increases with temperature to attain equilibrium.

It is also interesting to note the variation of  $\text{H}_2\text{O}$  concentration as a function of temperature with different inlet fuel compositions. For dry reforming (Fig. 1b), the species concentration is noted over-predicted in comparison with the reference data. The  $\text{H}_2\text{O}$  concentration computed with our model using the thermodynamic

analysis is maximum at around 750 K which is  $\approx 0.31\%$  and for reference results  $\approx 0.18\%$ . Whereas, for  $H_2$  co-feed (Fig. 5b), the peak for the present case is shifted towards higher temperature compared to the reference profile. This peak is still over-predicted with our model, however, the difference is small compared to the methane reforming without any co-feed ( $\approx 0.8\%$  at 800 K for LOGEcat and  $\approx 0.6\%$  at 600 K for reference case).

Delgado et al. [23] showed that for  $H_2O$  co-feed, Fig. 6b, the  $H_2O$  species is being consumed in temperature range 400–800 K showing a minimum concentration of the species at 900 K, i.e.,  $\approx 0.9\%$  and for the temperatures above 900 K, the formation of this species is seen. However, the computed species concentration with the thermodynamic model using the new surface reaction mechanism shows deviation in comparison with the reference profile. For our case, the species is formed in temperature range 400–700 K and then it is consumed until 1000 K followed by the formation of the species at higher temperature. Nonetheless, the behaviour of the profile is qualitative similar starting from 700 K when compared to the reference results.

Note that the production of hydrogen is increased for the DR process with additional co-feed,  $H_2$  as well as  $H_2O$ . The CO gas-phase species formation is reduced with additional inlet gases in DR and is seen minimum with  $H_2O$  as co-feed indicating the importance of hydrogen and water on DR.

The sensitivity analysis for formation of carbon, C(s), during dry reforming in the presence of  $H_2$  and  $H_2O$  at 1123 K is described in Fig. 7. Note that we have a different set of reactions which are most sensitive towards carbon formation with the kinetically consistent developed surface reaction mechanism as compared to the reactions mentioned in the reference paper [23]. Nevertheless, the reaction set for both the cases considered, DR with additional  $H_2$  (R5, R7, R24, R11, R19, R16, R8 and R23) as well  $H_2O$  (R24, R11, R7, R5 and R8), remains almost same with some extra reactions (less sensitive) noted in the former case. The most sensitive reaction for adding  $H_2$  are R5, R7 and R24, whereas for adding  $H_2O$  are R25, R11 and R7.

For a better understanding, we have summarised the most sensitive reactions in the reforming processes considered in this paper in Table 3 for the thermodynamic model developed in this work along with the kinetic model from Delgado et al. [23]. The common reactions found in both the models are highlighted in blue color in the table. Note that the sensitive reactions summarised for the DR process are same as for Fig. 4 whereas for DR with hydrogen and water as co-feed are same as Fig. 7. The differences in the sensitivity analysis are noticeable in DR with co-feed gases.

## Conclusions

A thermodynamic model is used to investigate dry reforming of methane over nickel catalyst. The model is applicable for modeling the other reforming processes as well, for instance, steam reforming (SR) and catalytic partial oxidation (CPOX) of methane over a nickel-based catalyst. However, in this paper our main aim is to understand the  $CO_2$  reforming and other reforming processes are discussed elsewhere.

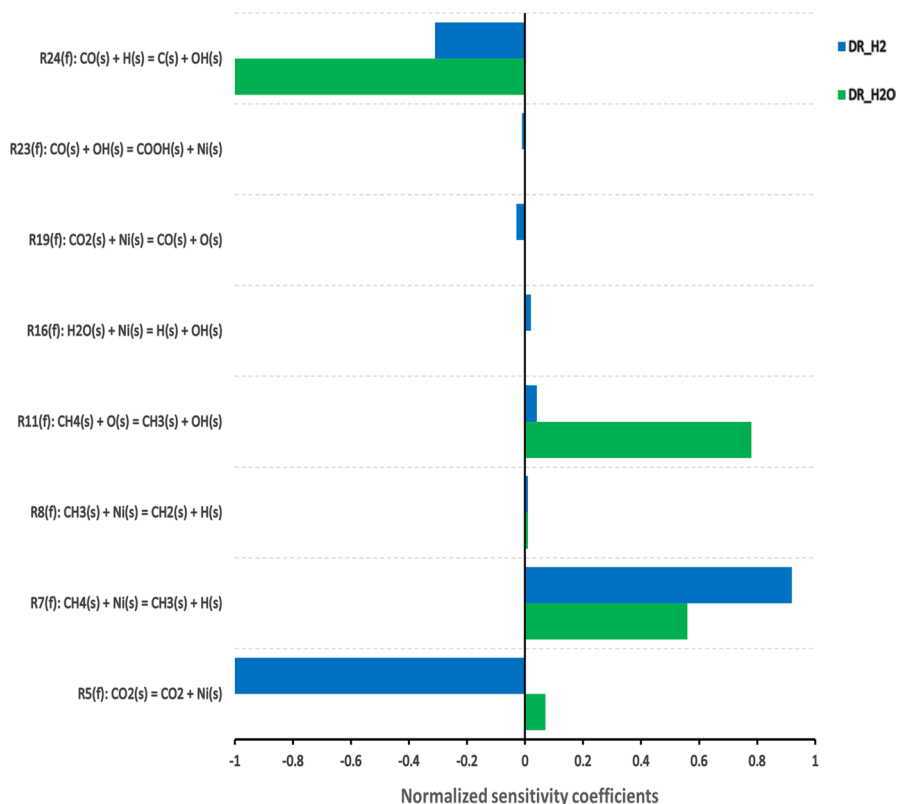


**Fig. 7** Sensitivity analysis for formation of carbon by DR in the presence of H<sub>2</sub> and H<sub>2</sub>O at 1123 K

The thermodynamic model is tested against literature experiments and simulations with the kinetic model from Delgado et al. [23] for DR and DR in the presence of hydrogen and water. The model is able to predict the reactants and products distribution for the whole temperature range considered for the simulations for dry reforming as well as with the co-feed of products, H<sub>2</sub> and H<sub>2</sub>O on the DR process over methane. However, a further investigation is recommended to improve the concentration of the species under different conditions, for example, H<sub>2</sub>O concentration for DR and co-feed of H<sub>2</sub> and H<sub>2</sub>O on the DR process.

The focus of the paper is also to perform a detailed sensitivity analysis for our reversible reactions or thermodynamic model considered in addition with the reaction flow analysis at various conditions. This is done to understand the carbon formation process for dry reforming with a thermodynamic model and to report the differences in the reaction pathways between the thermodynamic model and the kinetic schemes from literature. This helps us to understand the role of thermochemistry of the intermediate species in coke formation process.

**Table 3** Summary of the most influencing reactions in DR process as well as DR in the presence of H<sub>2</sub> and H<sub>2</sub>O for kinetic model from Delgado et al. [23] and thermodynamic model (this work). The simulating conditions are same as for Fig. 4 for DR and as Fig. 7 for the other two cases. The common reactions for both the models are highlighted in blue color in the table

Case	Kinetic model	Thermodynamic model
DR	$\text{CH}_4 + \text{Ni(s)} \rightarrow \text{CH}_4\text{(s)}$	
	$\text{CH}_4\text{(s)} + \text{Ni(s)} \rightarrow \text{CH}_3\text{(s)} + \text{H(s)}$	$\text{CH}_4\text{(s)} + \text{Ni(s)} = \text{CH}_3\text{(s)} + \text{H(s)}$
	$\text{CH}_4\text{(s)} + \text{O(s)} \rightarrow \text{CH}_3\text{(s)} + \text{OH(s)}$	$\text{CH}_4\text{(s)} + \text{O(s)} = \text{CH}_3\text{(s)} + \text{OH(s)}$
	$\text{CH}_4\text{(s)} \rightarrow \text{CH}_4 + \text{Ni(s)}$	
	$\text{CO}_2 + \text{Ni(s)} \rightarrow \text{CO}_2\text{(s)}$	
DR_H <sub>2</sub> O	$\text{CO(s)} + \text{H(s)} \rightarrow \text{C(s)} + \text{OH(s)}$	$\text{CO(s)} + \text{H(s)} = \text{C(s)} + \text{OH(s)}$
	$\text{CO}_2\text{(s)} + \text{Ni(s)} \rightarrow \text{CO(s)} + \text{O(s)}$	$\text{CH}_4\text{(s)} + \text{Ni(s)} = \text{CH}_3\text{(s)} + \text{H(s)}$
	$\text{OH(s)} + \text{Ni(s)} \rightarrow \text{H(s)} + \text{O(s)}$	$\text{CH}_4\text{(s)} + \text{O(s)} = \text{CH}_3\text{(s)} + \text{OH(s)}$
	$\text{C(s)} + \text{OH(s)} \rightarrow \text{CO(s)} + \text{H(s)}$	
	$\text{CO(s)} + \text{O(s)} \rightarrow \text{CO}_2\text{(s)} + \text{Ni(s)}$	
	$\text{H(s)} + \text{O(s)} \rightarrow \text{OH(s)} + \text{Ni(s)}$	
	$\text{CO}_2\text{(s)} \rightarrow \text{CO}_2 + \text{Ni(s)}$	
	$\text{CO(s)} + \text{H(s)} \rightarrow \text{C(s)} + \text{OH(s)}$	$\text{CO(s)} + \text{H(s)} = \text{C(s)} + \text{OH(s)}$
DR_H <sub>2</sub>	$\text{OH(s)} + \text{Ni(s)} \rightarrow \text{H(s)} + \text{O(s)}$	$\text{CH}_4\text{(s)} + \text{Ni(s)} = \text{CH}_3\text{(s)} + \text{H(s)}$
	$\text{C(s)} + \text{OH(s)} \rightarrow \text{CO(s)} + \text{H(s)}$	$\text{CO}_2\text{(s)} = \text{CO}_2 + \text{Ni(s)}$
	$\text{H(s)} + \text{O(s)} \rightarrow \text{OH(s)} + \text{Ni(s)}$	

**Acknowledgements** Financial support by the federal ministry of education and research (Bundesministerium für Bildung und Forschung, BMBF) under the Grant Number 03SF0693A of the collaborative research project “Energie-Innovationszentrum” is gratefully acknowledged.

**Funding** Open Access funding enabled and organized by Projekt DEAL.

**Open Access** This article is licensed under a Creative Commons Attribution 4.0 International License, which permits use, sharing, adaptation, distribution and reproduction in any medium or format, as long as you give appropriate credit to the original author(s) and the source, provide a link to the Creative Commons licence, and indicate if changes were made. The images or other third party material in this article are included in the article’s Creative Commons licence, unless indicated otherwise in a credit line to the material. If material is not included in the article’s Creative Commons licence and your intended use is not permitted by statutory regulation or exceeds the permitted use, you will need to obtain permission directly from the copyright holder. To view a copy of this licence, visit <http://creativecommons.org/licenses/by/4.0/>.

## References

1. Aparicio LM (1997) Transient isotopic studies and microkinetic modeling of methane reforming over nickel catalysts. *J Catal* 165:262–274. <https://doi.org/10.1006/jcat.1997.1468>
2. Rostrup-Nielsen JR, Sehested J, Nørskov JK (2002) Hydrogen and synthesis gas by steam- and CO<sub>2</sub> reforming. *Adv Catal* 47:65–139
3. Xu J, Froment GF (1989) Methane steam reforming, methanation and water-gas shift: I. Intrinsic kinetics. *Am Inst Chem Eng AIChE* 35:88–96. <https://doi.org/10.1002/aic.690350109>
4. Rostrup-Nielsen JR (2000) New aspects of syngas production and use. *Catal Today* 63:159–164

5. Rostrup-Nielsen JR (1984). In: Anderson JR, Boudart M (eds) Catalytic steam reforming in catalysis—science and technology. Springer, Berlin
6. Rostrup-Nielsen JR, Hansen JHB (1993) CO<sub>2</sub>-Reforming of methane over transition metals. *J Catal* 144:38–49. <https://doi.org/10.1006/jcat.1993.1312>
7. Bradford MCJ, Vannice MA (1999) CO<sub>2</sub> reforming of CH<sub>4</sub>. *Catal Rev* 41:1–42
8. Dissanayake D, Rosynek MP, Kharas KCC et al (1991) Partial oxidation of methane to carbon monoxide and hydrogen over a Ni/Al<sub>2</sub>O<sub>3</sub> catalyst. *Catal Today* 132:117–127. [https://doi.org/10.1016/0021-9517\(91\)90252-Y](https://doi.org/10.1016/0021-9517(91)90252-Y)
9. Zhu T, Flytzani-Stephanopoulos M (2001) Catalytic partial oxidation of methane to synthesis gas over Ni-CeO<sub>2</sub>. *Appl Catal A* 208:403–417
10. Tang S, Lin J, Tan KL (1998) Partial oxidation of methane to syngas over Ni/MgO, Ni/CaO and Ni/CeO<sub>2</sub>. *Catal Lett* 51:169–175
11. Vernon PF, Green MH, Cheetham A et al (1990) Partial oxidation of methane to synthesis gas. *Catal Lett* 6:181–186
12. Li C, Yu C, Shen S (2000) Role of the surface state of Ni/Al<sub>2</sub>O<sub>3</sub> in partial oxidation of CH<sub>4</sub>. *Catal Lett* 67:139–145
13. Rostrup-Nielsen JR (1984) Sulfur-passivated nickel-catalysts for carbon-free steam reforming of methane. *J Catal* 85:31–43
14. Trimm DL (1977) Formation and removal of coke from nickel-catalyst. *Catal Rev—Sci Eng* 16:155–189
15. Bartholomew CH (1982) Carbon deposition in steam reforming and methanation. *Catal Rev* 24:67–112
16. Blekkan EA, Myrstad R, Olsvik O et al (1992) Characterization of tars and coke formed during the pyrolysis of methane in a tubular reactor. *Carbon* 30:665–673
17. Wang S, Lu GQM (1998) CO<sub>2</sub> reforming of methane on Ni catalysts: Effects of the support phase and preparation technique. *Appl Catal B* 16:269–277
18. Chen D, Lodeng R, Anundskas A et al (2001) Deactivation during carbon dioxide reforming of methane over ni catalyst: microkinetic analysis. *Chem Eng Sci* 56:1371–1379
19. Chen D, Lødeng R, Svendsen H et al (2010) Hierarchical multiscale modeling of methane steam reforming reactions. *Ind Eng Chem Res* 50:2600–2612
20. Wei J, Iglesia E (2004) Isotopic and kinetic assessment of the mechanism of reactions of CH<sub>4</sub> with CO<sub>2</sub> or H<sub>2</sub>O to form synthesis gas and carbon on nickel catalysts. *J Catal* 224:370–383. <https://doi.org/10.1016/j.jcat.2004.02.032>
21. Blaylock DW, Ogura T, Green WH et al (2009) Computational investigation of thermochemistry and kinetics of steam methane reforming on Ni(111) under realistic conditions. *J Phys Chem A* 113:4898–4908
22. Iglesia E (1997) Design, synthesis, and use of cobalt-based fischer-tropsch synthesis catalysts. *Appl Catal A* 161:59–78
23. Delgado KH, Maier L, Tischer S et al (2015) Surface reaction kinetics of steam- and CO<sub>2</sub>-reforming as well as oxidation of methane over nickel-based catalysts. *Catalysts* 5:871–904. <https://doi.org/10.3390/catal5020871>
24. Rakhi, Shrestha KP, Günther V et al (2022) Kinetically consistent detailed surface reaction mechanism for steam reforming of methane over nickel catalyst. *React Kinet Mech Catal* 135:3059–3083. <https://doi.org/10.1007/s11144-022-02314-7>
25. Liu M, Dana AG, Johnson MS et al (2021) Reaction mechanism generator v3.0: advances in automatic mechanism generation. *J Chem Inf Model* 61:2686–2696. <https://doi.org/10.1021/acs.jcim.0c01480>
26. LOGEsoft (2008) V1.10 [www.logesoft.com](http://www.logesoft.com)

**Publisher's Note** Springer Nature remains neutral with regard to jurisdictional claims in published maps and institutional affiliations.